JPPIPA 12(10) (2026)

Jurnal Penelitian Pendidikan IPA

http://jppipa.unram.ac.id/index.php/jppipa/index

Design and Computer-Aided Chemical Calculations of Hetero ring Containing Acceptor-Typed Compounds

Abdul Manan Zahir[1*], Zainullah Matin[1], Abdul Jamil Haidari[2]

[1] Department of Food Engineering, Faculty of Industrial Chemical Engineering, Jawzjan University, Sheberghan, Afghanistan.
[2] Department of Inorganic Material Industry, Faculty of Industrial Chemical Engineering, Jawzjan University, Sheberghan, Afghanistan.

Received: September 10, 2026
Revised: October 21, 2026
Accepted: October 29, 2026
Published: October 31, 2026

Corresponding Author:
Abdul Manan Zahir
ustadmanan2018@gmail.com

DOI: 10.29303/jppipa.v12i10.16416

Open Access

© 2026 The Authors. This article is distributed under a (CC-BY License)

Abstract: Fullerene-free acceptors containing heterocycles are promising organic layers for photovoltaic devices, because the power conversion efficiency (PCE) of fullerene-free organic solar cells is higher than that of fullerene-based cells. In this study, banana-shaped, fullerene-free acceptor molecules (M1–M5) with a donor–acceptor–donor structure were designed by attaching conjugated triphenylamine groups to a 1,2,4-triazole core, building on furan-substituted triazole compounds previously synthesized and studied computationally by our group. Computer-aided chemical calculations used density functional theory (DFT) at the B3LYP/6-31G(d,p) level, and excited-state energies were obtained by time-dependent DFT within the Tamm–Dancoff approximation in the gas phase, chloroform, and dimethyl sulfoxide. The most stable conformers of all molecules adopted a banana-shaped geometry. Triphenylamine doping reduced the calculated HOMO–LUMO band gap relative to the parent compounds (for example, from about 3.9 eV for compound 1 to 2.62 eV for M1), while solvent polarity had little effect on the band gaps or frontier-orbital distributions. These results provide a theoretical basis for synthesizing the designed molecules and testing them in organic solar cells.

Keywords: Acceptor-typed compounds; Chemical calculations; Hetero ring; Triazole; PCE

Introduction

An electron acceptor is a molecule that receives electrons from a donor. In donor–acceptor systems, π-bridges in fullerene or non-fullerene motifs facilitate intramolecular charge transfer, generating redox interactions essential for efficient electron transport in optoelectronic devices (Rezvan, 2025).

Small-molecule non-fullerene acceptors (SMAs) attract strong interest in organic solar cells due to tunable energy levels and broad absorption, delivering higher efficiencies and improved photovoltaic performance compared with conventional fullerene-based acceptors (Yuan, Luo, Xie, & Peng, 2025).

Side-chain engineering effectively optimizes optoelectronic properties in organic solar cells. The Y6-derived acceptor BTSi-4F, incorporating a bulky siloxane-terminated side chain, shows improved solubility, elevated LUMO level, enhanced molecular packing, and higher electron mobility. PM6:BTSi-4F devices reached 16.6% PCE, with a Voc of 0.90 V and FF of 0.77, outperforming PM6:Y6(Yin et al., 2022).

Organic solar cells have progressed through ladder-type fused-ring NFAs, achieving high power conversion efficiencies, but their complex synthesis and high cost hinder large-scale use. Non-fused ring acceptors provide simpler structures, easier fabrication, and balanced efficiency. Recent studies emphasize molecular design, structure–property–performance relationships, device optimization strategies, and challenges guiding future material development (Yang, Wei, Zhou, Wang, & Duan, 2022; Zhang, Yuan, Wei, & Zou, 2018).

How to Cite:
Zahir, A. M., Matin, Z., & Haidari, A. J. (2026). Design and Computer-Aided Chemical Calculations of Hetero ring Containing Acceptor-Typed Compounds. *Jurnal Penelitian Pendidikan IPA*, *12*(10), 543–557. https://doi.org/10.29303/jppipa.v12i10.16416

Organic solar cells (OSCs) are attractive for next-generation photovoltaics because of their flexibility, light weight, and low-cost fabrication. Fused-ring non-fullerene acceptors have significantly improved efficiencies. Notably, Prof. Yingping Zou's Y6, based on a benzothiadiazole core (Figure 1), achieved 15.7% PCE by enhancing electron mobility, broadening absorption, suppressing aggregation, and enabling efficient charge transport in thick active layers (Chen, 2019).

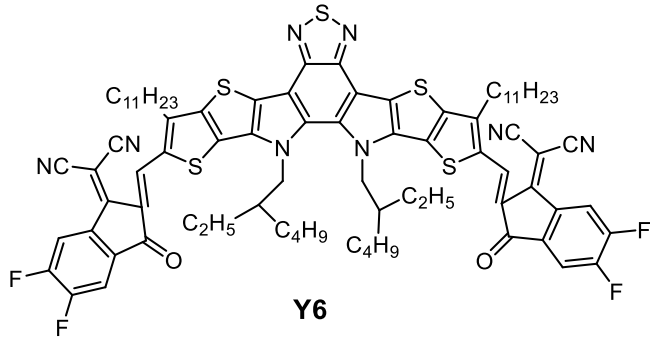


Figure 1. Molecular structure of the banana-shaped acceptor Y6 (Chen, 2019).

Organic Solar Cells (OSCs)

Organic solar cells (OSCs) convert sunlight into electricity and offer advantages such as stability, long lifetime, low cost, and safety. Solar radiation varies daily, and atmospheric gases and clouds absorb, scatter, and reflect light, reducing photon energy. The remaining sunlight reaching OSCs is converted into electrical power (Demirci, 2021).

Historically, energy was mainly used for heating, but electricity and industrialization have made it essential to modern life. Population growth and widespread electrification have increased global energy demand, while pollution and limited fossil fuels highlight the need for sustainable solutions. Solar energy is an abundant renewable resource converted into electricity by photovoltaic cells, where absorbed light generates charge carriers. Advances in materials and device engineering have improved PV efficiency and stability, supporting integration into energy infrastructures and promoting solar power as a key low-carbon energy solution (Sharda & Singh, 2019; Silva, 2024).

Fullerene-free acceptor molecules in solar cells

In conventional organic solar cells (OSCs), fullerene derivatives are typically employed as electron acceptor materials (Kollár, Pohl, Poppe, & Kohári, 2014; J. Lee, Lee, Lee, & Chu, 2009). Fullerenes in organic solar cells suffer from weak absorption, instability, limited energy-level tunability, and voltage losses. Small-molecule non-fullerene acceptors overcome these drawbacks, enabling higher power conversion efficiencies, mechanical flexibility, lightweight devices, and lower fabrication costs, positioning NFAs as superior, cost-effective materials for high-performance organic photovoltaic technologies suitable for next-generation solar energy applications (Kollár et al., 2014).

Adding functional layers to non-fullerene acceptors (NFAs) extends absorption into the near-infrared (NIR) region, while halogenation enhances charge transfer, molecular interactions, and packing, improving device performance (Aboulouard et al., 2021; Chen & Xu, 2018; Eok Jang, Ok Jeon, Joo Cho, Soo Yook, & Yeob Lee, 2010; Liu et al., 2020; Mahmood et al., 2018; Nielsen, Holliday, Chen, Cryer, & McCulloch, 2015; Zhao et al., 2020).

In organic solar cells, fluorine or chlorine incorporation into NFA backbones enables high-performance near-infrared absorption. As shown in Figure 2, non-covalent interactions (F•••H, F•••S) enhance molecular packing, maintain backbone planarity, and improve charge carrier mobility, boosting device efficiency (Hou, Inganäs, Friend, & Gao, 2018; R. Xie et al., 2018).

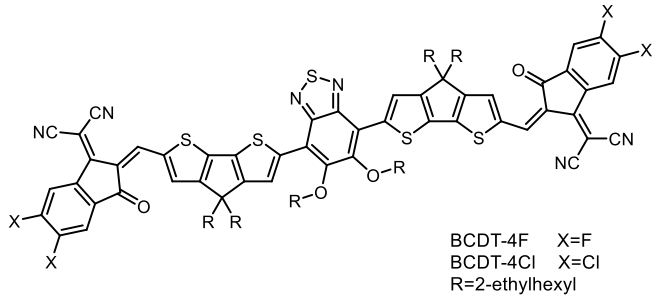


Figure 2. Molecular structure of BCDT-4X with simplified side chains

Figure 2 presents NIR acceptors BCDT-4F and BCDT-4Cl with an A–D–C–D–A architecture. Bulky-free side groups and noncovalent interactions stabilize geometry, while BT units tune HOMO levels, enhance charge transfer, narrow bandgaps, and enable higher PCE and current density for PBDB-T:BCDT-4Cl devices in OSCs (He et al., 2020).

Small acceptor molecules with Ladder-shaped alkyl side chains

Figure 3 illustrates Y6, a pyrrole-based acceptor bearing nitrogen-linked alkyl chains. Branched 2-ethylhexyl groups occupy the 2-position on sp^2 nitrogens, while linear n-undecyl chains reside on outer-core thiophenes. Side-chain rearrangement produced N3, whose branched chain at the 3-position enhances morphology, crystallinity, face-on π–π stacking, and device efficiency, reaching a PCE of 16.42% in OSCs.

Ultimately, the best device performance was achieved with N3, delivering a power conversion efficiency (PCE) of 16.0% (Jiang et al., 2019).

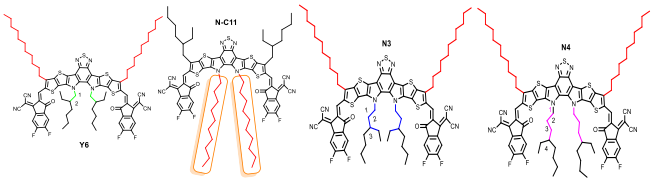


Figure 3. Molecular structures of Y6, NC11, N3, and N4

Figure 3 depicts Y6, a Y-series non-fullerene acceptor with a planar fused-aromatic core enabling broad NIR absorption and efficient charge transport. Its alkyl side chains regulate molecular packing, phase separation, thin-film morphology, and charge-transport pathways, thereby enhancing OSC power conversion efficiency (Fu et al., 2023).

In Y6, branched chains on pyrrole nitrogens and linear chains on outer-core thiophenes balance solubility, crystallinity, and interactions. Changing their type or position shifts packing from edge-on to face-on π–π stacking, enhancing charge transport and device performance (Fürk et al., 2023).

Alkyl side-chain engineering in Y6 derivatives tunes active-layer morphology: branched chains reduce aggregation and uniformize donor–acceptor phases, linear chains increase crystallinity, and combining both enhances crystallinity and charge-transport networks, improving device performance (Xu et al., 2023).

Repositioning alkyl side chains in Y6 derivatives, such as N3, shifts the branched chain to a new site, significantly altering molecular orientation in thin films. This change promotes a dominant face-on alignment and shorter π–π stacking distance, enhancing vertical charge transport and improving device performance (Lei, Meng, Guo, Sun, & Zhou, 2025).

Small-molecule acceptors incorporating thieno[3,2-b]thiophene (TT) units

Thienothiophene (TT) is formed by the fusion of two five-membered heterocyclic rings and exists in four main structural isomers, namely thieno[3,2-b]thiophene (1), thieno[2,3-b]thiophene (2), thieno[4,3-b]thiophene (3), and 1H,3H-thieno[4,3-c]thiophene (4) (Demirci, 2021).

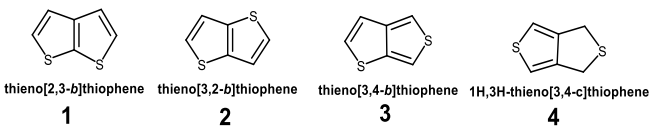


Figure 4. Thienothiophene Analogues

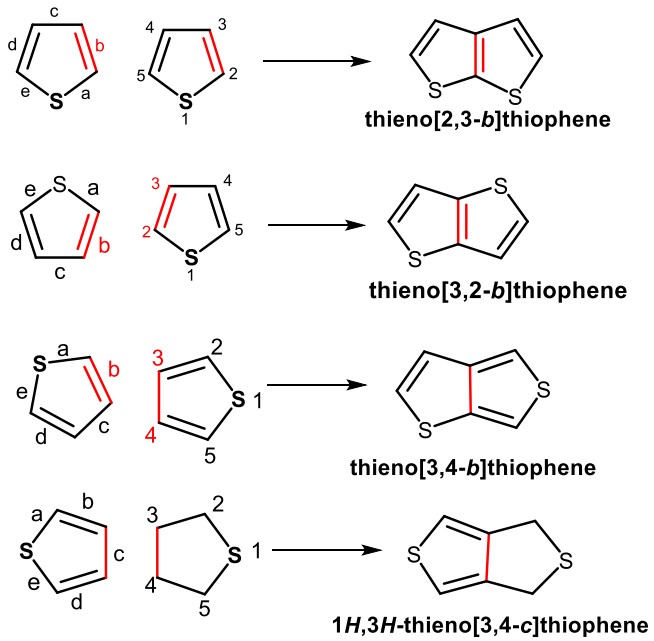


Figure 5. Schematic Nomenclature of thienothiophene Molecules

Wang et al. (2018) synthesized two multifunctional A–D–A photovoltaic materials, DRCN3TT and DRCN5TT, featuring a thieno[3,2-b]thiophene core and dicyanomethylene rodanine terminals. Their favorable energy levels and ambipolar charge transport allow them to act as both donors and acceptors, demonstrating multifunctional materials as a promising approach for high-performance organic solar cells (Wang et al., 2018).

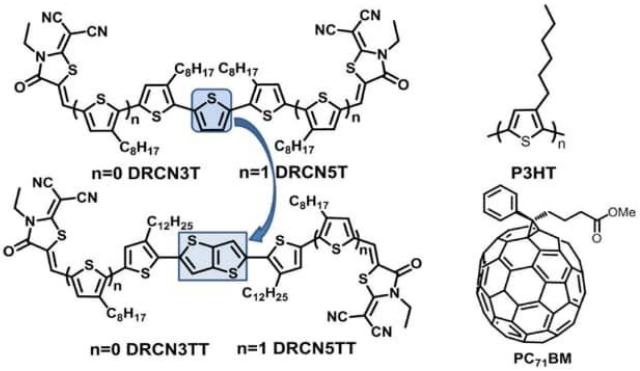


Figure 6. Molecular Structures of DRCN3T, DRCN5T, DRCN3TT, DRCN5TT, P3HT, and PC71BM

Xie et al. (2025) investigated side-chain engineering in small-molecule acceptors. The asymmetric BT-ASY, with branched alkyl chains and β-thiophene substitutions, achieved 18.08% PCE, surpassing symmetric BT-BO and BT-TBO. Improved mobility, packing, and phase separation show that asymmetric side chains enhance π–π interactions and solar cell efficiency (Xie et al., 2025).



Figure 7. Molecular Structures of BT-BO, BT-TBO, and BT-ASY

Li et al. (2026) developed the non-fused ring electron acceptor TT Ph C6 with asymmetric side chains, outperforming symmetric 2BTh-2F. Its dense crystalline packing and strong π–π interactions enhance electron mobility and exciton diffusion. Devices achieved 18.01% PCE and 80.10% FF at 100 nm, maintaining high efficiency at 200–300 nm, demonstrating asymmetric side-chain design as a cost-effective strategy for high-performance NFREAs(Li et al., 2026).

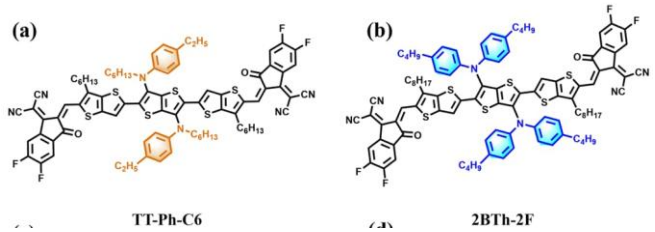


Figure 8. Chemical structures of the electron acceptors (a) TT Ph C6 and (b) 2BTh-2F

Triphenylamine-containing molecules used in solar cells

Molecules with a D–π–A architecture and a triphenylamine (TPA) core function as efficient electron donors. Rajavelu and Rajakumar (2018) synthesized stilbenoid dendrimers combining a TPA donor and benzothiazole acceptor with high yields. Extended π-conjugation enhanced light absorption and harvesting, while cyclic voltammetry showed quasi-reversible TPA oxidation. Using these dendrimers as DSSC additives improved performance, with one achieving 5.08% PCE (Rajavelu & Rajakumar, 2018).

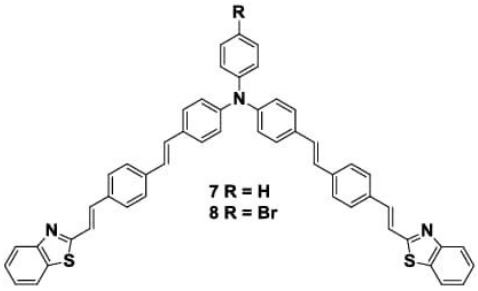


Figure 9. Chemical structure of star-shaped triphenylamine-based conjugated molecules

Wang, Chen, Xu, and Ji (2010) synthesized π-conjugated compounds with triphenylamine donors and benzothiazole acceptors to study donor–acceptor ratio effects on optical properties. DFT calculations showed optimized geometries and HOMO/LUMO distributions. The compounds displayed high molar absorption, strong quantum yields, thermal stability, and blue–green emission, indicating potential for OLEDs (Wang et al., 2010).

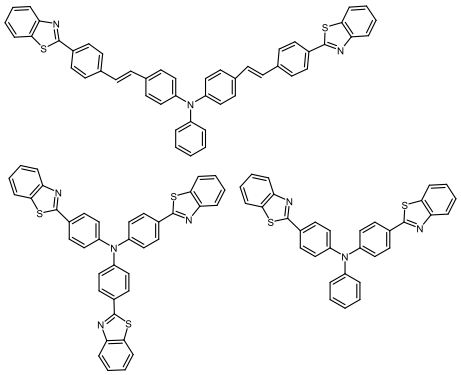


Figure 10. Y-shaped and star-shaped π-conjugated molecular structures

Mahmoud, Badawy, Fadda, Abdel-Latif, and Elmorsy (2025) designed metal-free D–π–A dyes based on triphenylamine (TPA) (Figure 11) with extended visible-light absorption. Experimental and theoretical studies showed that combining these dyes with N-719 significantly improved DSSC efficiency. Among them, SAS-2 achieved the highest PCE of 9.12%, highlighting the strong potential of TPA-based dyes to enhance DSSC performance (Mahmoud et al., 2025).

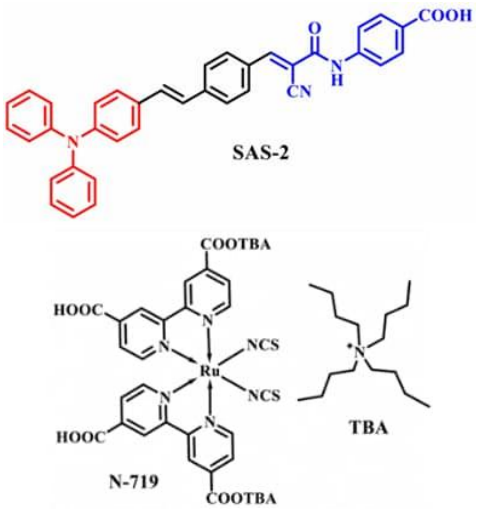


Figure 11. Molecular structures of the metal-free organic dye SAS-2 and the ruthenium polypyridyl sensitizer N-719 used in dye-sensitized solar cells

Quezada-Borja et al. (2022) designed ten triphenylamine (TPA)-based molecules with five p-linkers as hole transport materials (HTMs) for

perovskite solar cells. DFT and DFTB calculations revealed higher HOMO levels than perovskite, occasionally surpassing Spiro-OMeTAD, confirming their effectiveness as efficient HTMs (Quezada-Borja et al., 2022).

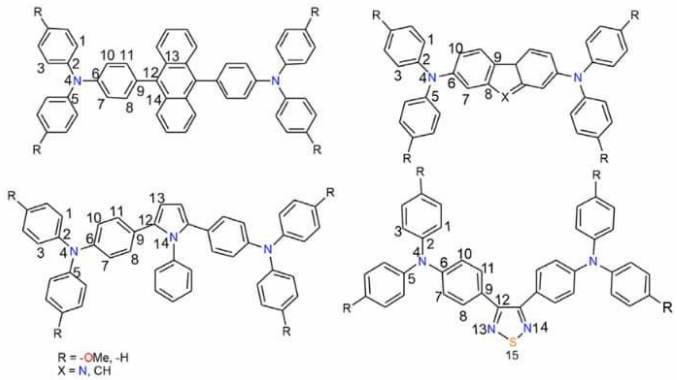


Figure 12. Atom numbering scheme in triphenylamine derivatives.

Park et al. (2016) synthesized [2,2] paracyclophane-based HTMs with multiple triphenylamine (TPA) units. Increasing TPA arms improved charge transfer in the amorphous HTM layer, enhancing perovskite solar cell performance. Tetra-TPA devices achieved higher short-circuit current, fill factor, and a PCE of 17.9%, surpassing di-TPA and tri-TPA cells (Park et al., 2016).

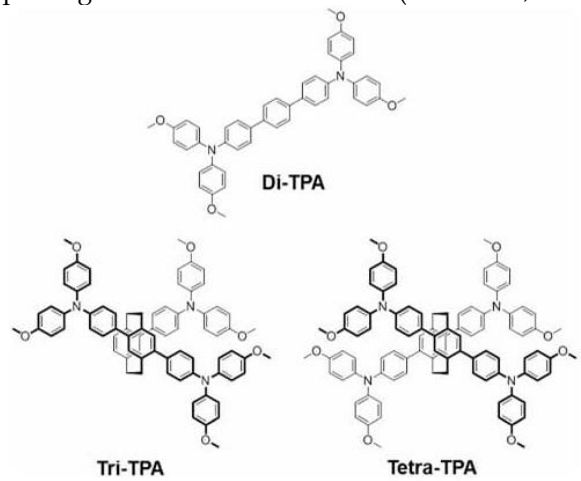


Figure 13. Structures of HTMs containing two, three, and four TPAs incorporated into a [2,2]paracyclophane core.

Method

A triazole-containing molecule

Triazole is a highly important heterocyclic compound that exhibits remarkable pharmacological activities across diverse species and structural frameworks. This ring system is an unsaturated five-membered heterocycle containing three nitrogen atoms. As illustrated in Figure 14, triazole exists in two isomeric forms, namely 1,2,3-triazole and 1,2,4-triazole.

Triazoles, particularly benzo[d][1,2,3]triazole (BTA), constitute an important class of heterocyclic compounds that are widely employed in the design of non-fullerene acceptor molecules for organic solar cells, owing to their strong electron-withdrawing characteristics and their ability to absorb light in the visible to near-infrared (Vis/NIR) region. Specifically, BTA functions as a central unit or active building block within the A–D–A molecular architecture, leading to enhanced charge transport and broader spectral absorption (J. E. Lee et al., 2021).

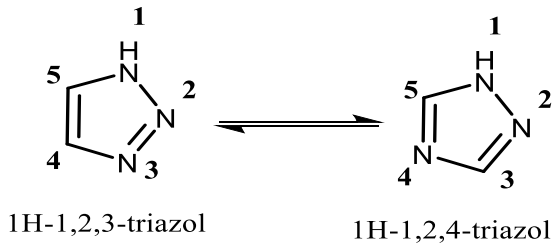


Figure 14. Isomers of triazole

In 2019, our research group synthesized a series of furan-substituted 1,2,4-triazole–based compounds to evaluate their potential application in solar cell technologies. Computational chemical calculations were also performed to investigate their electronic properties. The study demonstrated that doping these compounds with conjugated functional groups can effectively reduce the band gap energy (Akış, 2019).

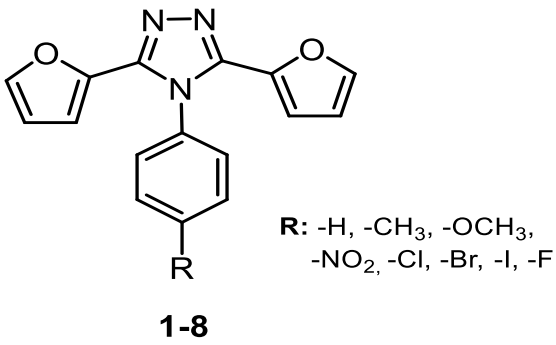


Figure 15. Chemical structures of compounds 1–8 were synthesized in the previous study.

Based on this background, the present study involved the design of various molecules by increasing the degree of conjugation in furan-linked 1,2,4-triazole–based compounds. Computational chemical calculations were carried out for the designed molecules, and their electron transition energies were systematically investigated.

To construct a conjugated donor–acceptor–donor (D–A–D) architecture, an electron-donating unit, triphenylamine, was attached to the 5-position of each

furan ring in the corresponding compounds. Following geometric optimization of each studied molecule (M1–M5), the computational analyses were performed based on the three lowest-energy conformations obtained.

This study is founded on the design of molecules M1–M5 and the theoretical execution of computational chemical calculations. The computational procedure began with relatively simple methods and was progressively advanced toward more sophisticated and complex approaches. For the quantum chemical calculations, the Gaussian 16 Rev. A.03 software package (Frisch, 2019) was employed. This program is widely recognized as one of the most extensively used tools for investigating molecular structural characteristics, spectroscopic properties, electronic features, and nonlinear optical properties.

The results obtained from these calculations enable detailed analysis of both molecular and atomic properties, including molecular orbital energies, atomic charges, ionization energies, electrostatic potentials, spin densities, and electron density maps (Foresman & Frisch, 1993). These data allow researchers to comprehensively evaluate molecular structures and properties, thereby achieving a deeper understanding of their chemical behavior.

Geometric structural analyses of the molecules were carried out using the ChemAxon Marvin Suite software (ChemAxon, 2019). In addition, the ChemOffice software package (PerkinElmer, 2021) was employed to transfer the molecules into a digital environment and to perform molecular mechanics calculations. These programs enable detailed examination of molecular geometries and the stability of different conformations, thereby providing a reliable foundation for subsequent quantum chemical calculations and further analyses.

GaussView 6.0.16 is a graphical user interface widely used for three-dimensional molecular modeling, preparation of input files for the Gaussian 16 Rev. A.03 program (Frisch, 2019) and visualization of computational results. Using this software, researchers can accurately examine the three-dimensional structures of molecules, bond lengths, bond angles, and other molecular graphical properties, enabling informative visual analyses based on quantum chemical calculations.

All calculations conducted in this study were performed using two computing platforms. The first was a Lenovo IdeaPad personal laptop equipped with a GeForce GTX graphics card, an AMD Ryzen 7 processor (3.8 GHz), 16 GB of RAM, a 64-bit operating system, eight processing cores, and Windows 10 Home Single Language. The second system was a desktop computer powered by an Intel Core i7 Extreme 3970X processor (3.50 GHz) with six cores (12 threads), 64 GB (8 × 8 GB) DDR3 1333 MHz RAM, and an Intel X79 LGA2011 chipset. The use of these systems enabled the efficient performance of demanding quantum chemical calculations and complex molecular analyses.

Using computational approaches, geometric optimization, frequency calculations, and excited-state energy calculations were sequentially performed for molecules M1–M5 in both the gas phase and solvent phase. Because experimental synthesis requires knowing which solvents will dissolve the molecules, it is necessary to predict the solvents in which these molecules would be soluble, additional calculations were carried out in relevant solvent environments. In the quantum chemical calculations, chloroform ($CHCl_3$) and dimethyl sulfoxide (DMSO) were selected as the model solvents.

The computational results provided the maximum absorption wavelengths (λmax), electron transition percentages (T), band gap energies (Egap), dipole moments, and the sums of electronic and thermal free energies (ΔG) for molecules M1–M5.

Molecular Geometry Optimization

Molecular geometry optimization is used, in simple terms, to obtain the molecular structure with the lowest possible energy. Mathematically, this means that the first derivative of the energy with respect to atomic coordinates (the gradient) is zero, while the second derivative (the force constant) is positive. In this study, the potential energy surface (PES) scan method was employed to determine the most stable conformations of molecules M1–M5. Based on the data obtained from this analysis, three of the most stable geometries were selected for each molecule, and all subsequent calculations were performed on these optimized structures.

These calculations were performed using the hybrid Density Functional Theory (DFT) method, B3LYP, which simultaneously employs the B3 exchange functional and the LYP correlation functional. In these computations, the 6-31G(d,p) basis set was selected as the basis for all atoms.

Result and Discussion

Frequency Calculations

After performing potential energy surface scans for molecules M1–M5, data corresponding to the three lowest-energy conformations for each compound were extracted in both the gas phase and the selected solvents. These data included dipole moments, free energies, atomic partial charges, and vibrational frequencies, all obtained from the output (.log) files of the frequency calculations conducted following the molecular geometry optimization.

Table 1. Calculated Values of Dipole Moment and Total Electronic and Thermal Free Energies for Molecules M1–M5

Molecule	Solvent	ΔG (kcal/mol)	Dipole moment (Debye)
	Gas	-2427.38	5.61
M11	$CHCl_3$	-2427.40	7.40
	DMSO	-2427.40	8.03
	Gas	-2427.38	6.11
M12	$CHCl_3$	-2427.40	8.06
	DMSO	-2427.40	8.95
	Gas	-2427.38	6.40
M13	$CHCl_3$	-2427.40	8.01
	DMSO	-2427.40	9.45
	Gas	-2466.70	6.24
M21	$CHCl_3$	-2466.66	7.20
	DMSO	-2466.70	8.71
	Gas	-2466.68	6.56
M22	$CHCl_3$	-2466.70	8.60
	DMSO	-2466.70	9.65
	Gas	-2466.68	6.80
M23	$CHCl_3$	-2466.67	9.23
	DMSO	-2466.70	10.14
	Gas	-2886.98	3.56
M31	$CHCl_3$	-2888.00	5.00
	DMSO	-2887.00	5.55
	Gas	-2886.98	4.42
M32	$CHCl_3$	-2887.00	5.95
	DMSO	-2887.00	6.51
	Gas	-2886.99	5.08
M33	$CHCl_3$	-2887.00	6.60
	DMSO	-2887.00	7.15
	Gas	-2526.62	4.06
M41	$CHCl_3$	-2526.61	7.12
	DMSO	-2526.64	6.29
	Gas	-2526.62	4.86
M42	$CHCl_3$	-2526.61	6.50
	DMSO	-2526.65	7.21
	Gas	-2526.62	5.33
M43	$CHCl_3$	-2526.63	7.17
	DMSO	-2526.64	7.80
	Gas	-4998.49	3.69
M51	$CHCl_3$	-4998.51	5.20
	DMSO	-4998.52	5.74
	Gas	-4998.50	4.65
M52	$CHCl_3$	-4998.51	6.20
	DMSO	-4998.52	6.77
	Gas	-4998.50	4.64
M53	$CHCl_3$	-4998.51	6.70
	DMSO	-4998.52	7.55

Prior to performing excited-state energy calculations, the free energies of the corresponding molecular conformations were evaluated, revealing that the first conformer represents the most stable structure for each compound. As previously noted, earlier studies have reported that some electron-acceptor molecules exhibit a bent, "banana-shaped" geometry in their conformational analyses. Similarly, it was observed that the most stable first conformers of molecules M1–M5 also adopt this characteristic banana-shaped curvature, whereas the other conformers do not display such spatial arrangements.

To determine the charge distribution and reactive sites of the designed molecules, the molecular charge distribution (Mulliken charges) was calculated for all conformers. These calculations are highly valuable for the design and modification of new molecules in future studies.

In the Mulliken charge distribution, the color of each atom represents its partial charge. Green-colored atoms exhibit higher electropositive character, whereas red-colored atoms are more electronegative. Specifically, the red atoms are primarily nitrogen and oxygen, while the groups attached to these atoms are generally green, indicating a slight increase in positive charge density in these regions. Atoms colored near black are essentially neutral and are expected to show lower reactivity in these areas.

Next, the two-dimensional and three-dimensional structures of the molecules, along with the Mulliken charge distributions, are presented for the most stable conformers of M1–M5. The charge distributions of the other conformers of these molecules can be found in Appendix EK-5.

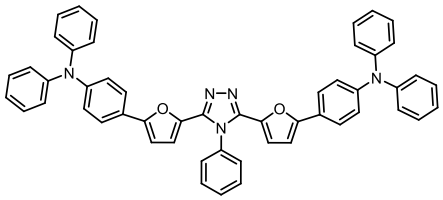


Figure 16. 4,4′-((4-Phenyl-4H-1,2,4-triazole-3,5-diyl)bis(furan-5,2-diyl))bis (N,N-diphenylaniline)



Figure 17. Three-Dimensional Structure of the First Conformer (M11) of Molecule M1

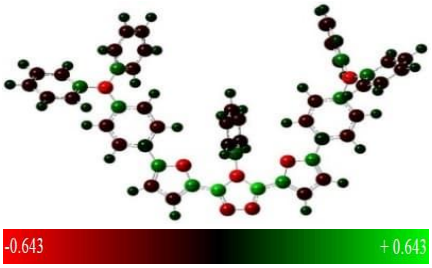


Figure 18. Mulliken Charge Distribution of Conformer M11

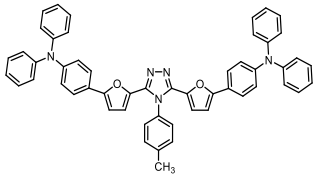


Figure 19. 4,4′-((4-(p-Tolyl)-4H-1,2,4-triazole-3,5-diyl)bis(furan-5,2-diyl))bis (N,N-diphenylaniline)

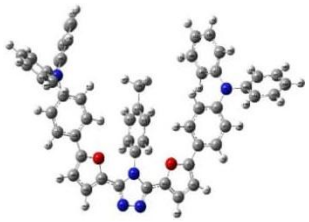


Figure 20. Three-Dimensional Structure of the First Conformer (M21) of Molecule M2

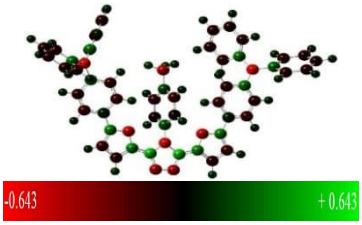


Figure 21. Mulliken Charge Distribution of Conformer M21

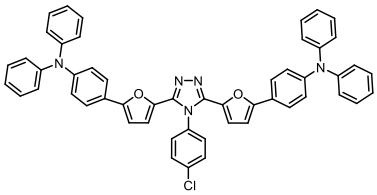


Figure 22. 4,4′-((4-(4-Chlorophenyl)-4H-1,2,4-triazole-3,5-diyl)bis(furan-5,2-diyl))bis (N,N-diphenylaniline)

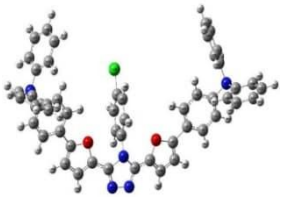


Figure 23. Three-Dimensional Structure of the First Conformer (M31) of Molecule M3

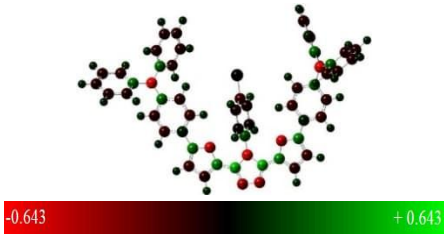


Figure 24. Mulliken Charge Distribution of Conformer M31

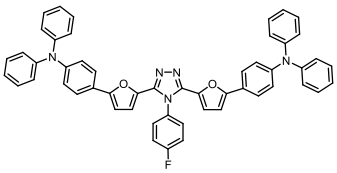


Figure 25. 4,4′-((4-(4-Fluorophenyl)-4H-1,2,4-triazole-3,5-diyl)bis(furan-5,2-diyl))bis (N,N-diphenylaniline)

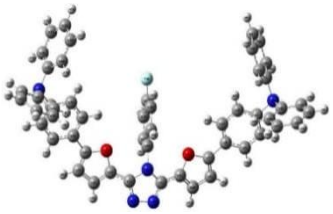


Figure 26. Three-Dimensional Structure of the First Conformer (M41) of Molecule M4

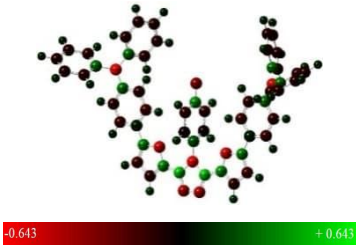


Figure 27. Mulliken Charge Distribution of Conformer M41

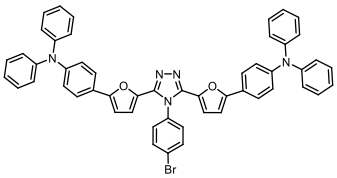


Figure 28. 4,4′-((4-(4-Bromophenyl)-4H-1,2,4-triazole-3,5-diyl)bis(furan-5,2-diyl))bis (N,N-diphenylaniline)



Figure 29. Three-Dimensional Structure of the First Conformer (M51) of Molecule M5

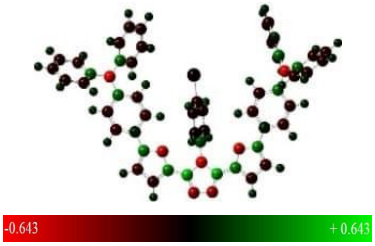


Figure 30. Mulliken Charge Distribution of Conformer M51

Excited-State Energy Calculations

The vertical excitation energies of the molecules were calculated using the Tamm-Dancoff approximation (TD-DFT/TDA) within the framework of time-dependent density functional theory (TD-DFT), employing the B3LYP/6-31G(d,p) basis set. Table 2 presents the results of the excited-state energy calculations for molecules M1–M5, including the maximum absorption wavelengths (λmax), electron transition percentages (T), and band gap energies (Egap).

Table 2. Calculated Values of Wavelengths (λ), Electron Transition Percentages (T), and Band Gap Energies (Egap) for Molecules M1–M5

Molecule	Solvent	λ (nm)	T (%)	Egap (eV)
M11	Gas	426.14	96.08	2.91
	CHCl3	437.96	95.44	2.83
	DMSO	439.03	95.44	2.82
M12	Gas	430.09	95.87	2.85
	CHCl3	463.83	97.07	2.67
	DMSO	439.03	95.44	2.82
M13	Gas	434.88	96.56	2.85
	CHCl3	446.33	96.44	2.78
	DMSO	447.69	96.45	2.77
M21	Gas	425.19	96.05	2.92
	CHCl3	437.13	95.41	2.84
	DMSO	438.29	95.42	2.83
M22	Gas	429.42	95.75	2.89
	CHCl3	439.91	95.66	2.82
	DMSO	440.40	95.78	2.82
M23	Gas	432.62	96.50	2.87
	CHCl3	443.58	96.38	2.80
	DMSO	445.13	96.39	2.79
M31	Gas	429.19	96.16	2.89
	CHCl3	440.53	95.52	2.81
	DMSO	441.23	95.53	2.81
M32	Gas	433.21	96.04	2.86
	CHCl3	444.34	95.83	2.79
	DMSO	445.06	95.94	2.79

The changes in the maximum absorption wavelengths (λmax) for the most stable conformers of M1–M5 (M11, M21, M31, M41, M51) in different solvents were obtained from the excited-state energy calculations and UV–Vis spectra.

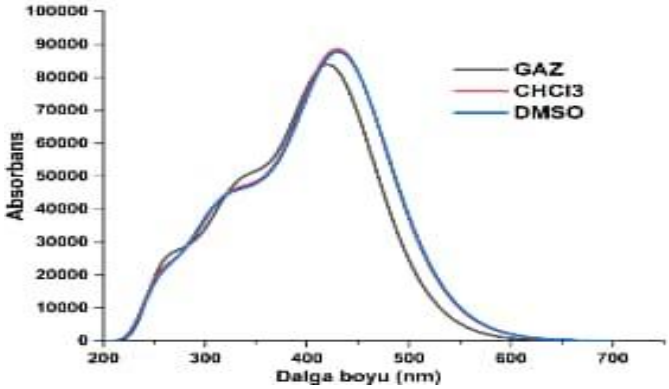


Figure 31. Calculated UV–Vis Spectra of Conformer M11

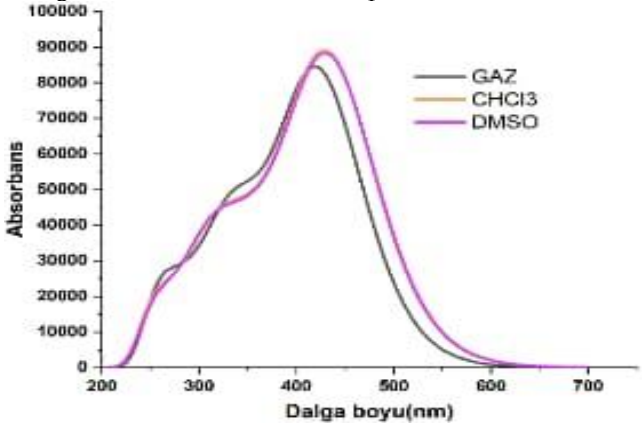


Figure 32. Calculated UV–Vis Spectra of Conformer M21

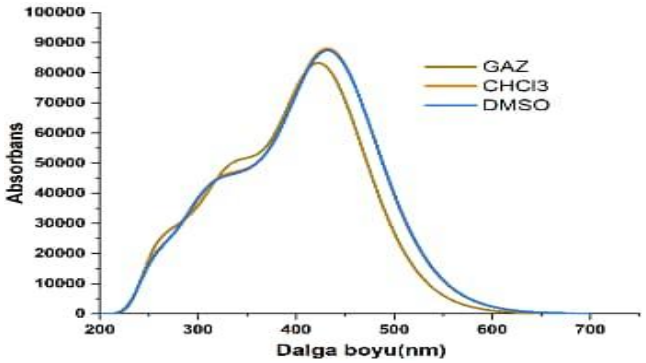


Figure 33. Calculated UV–Vis Spectra of Conformer M31

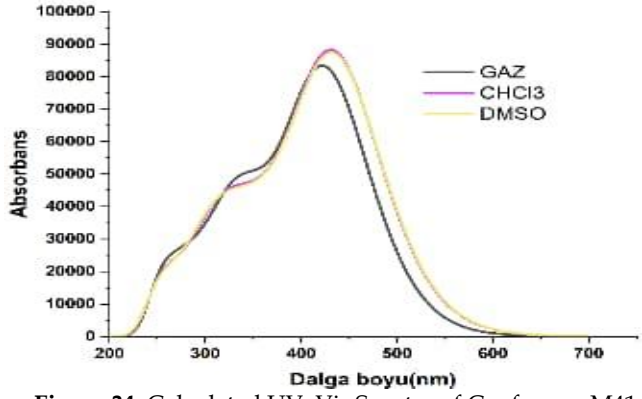


Figure 34. Calculated UV–Vis Spectra of Conformer M41

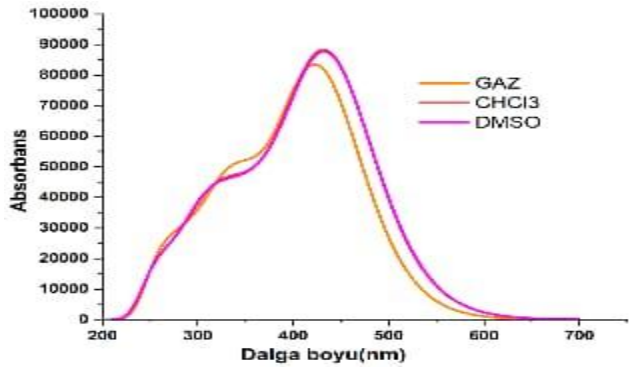


Figure 35. Calculated UV–Vis Spectra of Conformer M51

Compared to the gas-phase spectra obtained from the calculations, the spectra of the molecules in $CHCl_3$ and DMSO show a slight red shift of a few nanometers. However, when the spectra in these two solvents are compared with each other, no noticeable red shift is observed.

Using the results from frequency and excited-state energy calculations, the frontier orbitals (HOMO–LUMO) of the target molecules can be visualized. These frontier orbital images provide important information about the electron density distribution within the molecule and help identify charge-carrying groups. Accordingly, the frontier orbitals of the most stable conformers of M1–M5 in the gas phase and in $CHCl_3$ and DMSO solvents are presented in Figures 36 and 37.

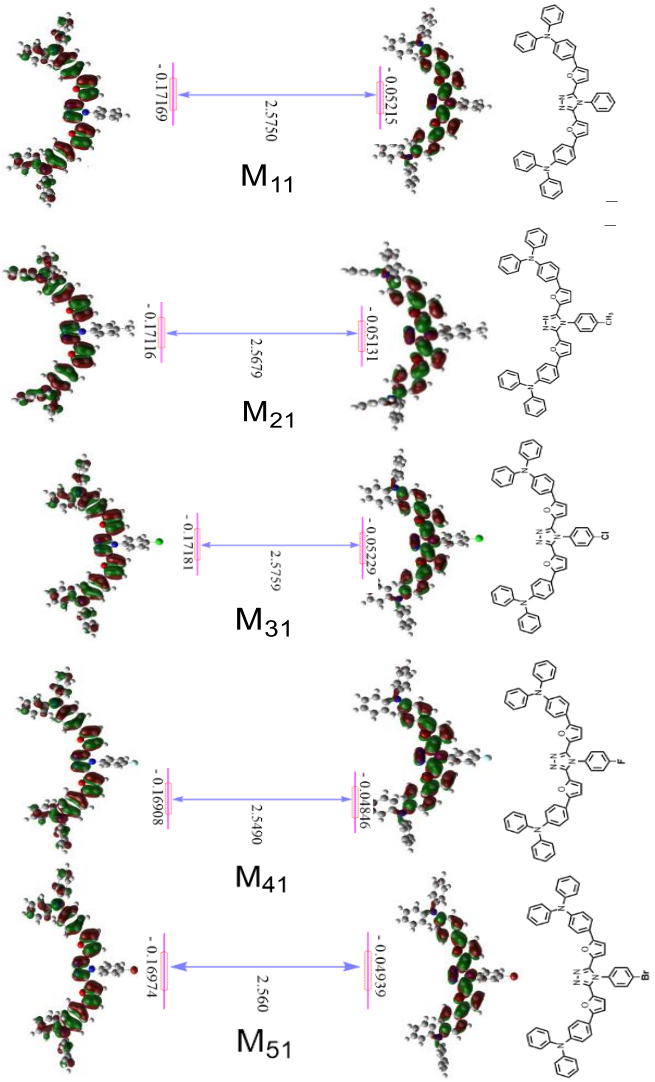


Figure 36. Frontier HOMO–LUMO orbitals and band gap energies of conformers M11 to M51 in the gas phase

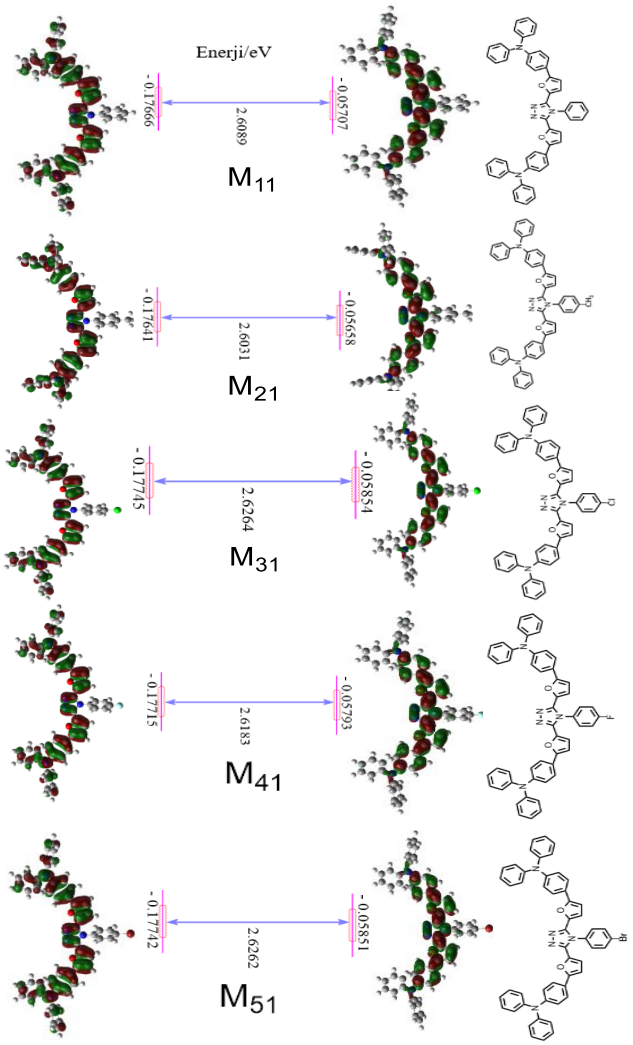


Figure 37. Frontier HOMO–LUMO orbitals and band gap energies of conformers M11 to M51 in DMSO phase

Discussion

In this study, 1,2,4-triazole was strategically selected as the central molecular core due to its remarkable combination of chemical stability, planarity, and electronic versatility. The intrinsic structural characteristics of 1,2,4-triazole render it an ideal scaffold for the development of conjugated organic systems, particularly in applications such as organic photovoltaics (OPVs), where efficient electron delocalization and structural robustness are critical. Its planar geometry promotes effective π-orbital overlap, which is essential for facilitating efficient π-conjugation between electron-donating and electron-accepting moieties. Furthermore, the synthetic accessibility of the triazole ring, along with its stability under a range of reaction conditions, provides a practical advantage for designing functional small molecules. Building upon these considerations, a series of small non-fullerene acceptor (NFA) molecules, denoted as M1 through M5, were rationally designed following a donor–acceptor–donor (D–A–D) architecture with the 1,2,4-triazole unit at their core.

The design of M1–M5 was informed by extensive prior research demonstrating that the molecular geometry of small NFAs can adopt a variety of shapes, including banana-shaped, ladder-type, and star-shaped conformations. Each of these structural motifs exerts a pronounced influence on key properties such as charge transport efficiency, molecular packing, and optical absorption. In particular, banana-shaped molecules have been reported to facilitate enhanced π–π stacking interactions, thereby improving intermolecular charge transport pathways. Given these insights, the triazole core was chosen not only for its capacity to support highly conjugated systems but also for its ability to maintain a stable molecular framework, which is essential for achieving reproducible electronic properties in NFAs. These attributes collectively render triazole a highly suitable candidate for the development of next-generation OPV materials.

To systematically investigate the structural and electronic characteristics of the designed molecules, comprehensive quantum chemical calculations were carried out using density functional theory (DFT) at the B3LYP/6-31G(d,p) level. Geometry optimizations and potential energy surface (PES) scans were performed to identify the most energetically favorable conformations. The results revealed that the lowest-energy geometries of M1–M5, hereafter referred to as M11–M51, adopt a distinctive banana-shaped configuration. This geometry is particularly advantageous for π–π stacking, a critical factor in promoting efficient charge transport and intermolecular electronic coupling in OPV devices. These findings indicate that the designed molecules possess intrinsic structural features conducive to high-performance photovoltaic behavior.

Our previous experimental investigations on furan-substituted 1,2,4-triazole derivatives (compounds 1–8) provided a valuable reference framework for evaluating the designed molecules. Comparative analyses between experimental measurements and computational predictions revealed close agreement in electronic properties such as frontier molecular orbital (FMO) energies and charge distribution patterns. However, it was noted that the experimental and calculated excited-state energy levels indicated relatively high HOMO–LUMO gaps, with the compounds exhibiting band gaps consistent with insulating or poorly semiconducting behavior. Given that efficient OPV materials require semiconducting characteristics with narrower band gaps to facilitate light absorption and charge separation, strategies were needed to reduce the electronic band gaps of the designed NFAs and optimize their photovoltaic potential.

Two principal molecular design strategies were considered to address this challenge. First, the incorporation of highly conjugated groups into the central molecular framework was proposed as a means to extend the delocalization of π-electrons. By increasing the extent of conjugation, the HOMO–LUMO gap could be effectively reduced, thereby enhancing charge delocalization and improving electronic conductivity. Second, the strategic attachment of electron-donating and electron-withdrawing chromophores was employed to induce a pronounced push–pull effect. This approach is well-known to facilitate intramolecular charge transfer, enhance optical absorption in the visible spectrum, and modulate electronic energy levels, all of which are critical for high-performance NFAs in OPVs.

Based on these rational design principles, compounds 1–5, initially conceptualized by Merve Akış, were subjected to electron injection through the incorporation of triphenylamine (TPA) donor groups. The TPA moiety was specifically chosen due to its strong electron-donating character, which effectively promotes π-conjugation throughout the molecular backbone. Computational analyses demonstrated that TPA functionalization led to a significant reduction in the HOMO–LUMO gap across all derivatives, confirming the efficacy of this strategy. For instance, compound 1 exhibited an experimental band gap of 3.66 eV and a calculated gap of 3.93 eV in DMSO prior to TPA incorporation. Following TPA functionalization, the resulting molecule, M1, displayed a reduced calculated band gap of 2.62 eV, highlighting a marked improvement in semiconducting behavior. Comparable trends were observed for M2–M4, indicating that TPA doping systematically enhances π-conjugation and modulates electronic properties in a predictable manner.

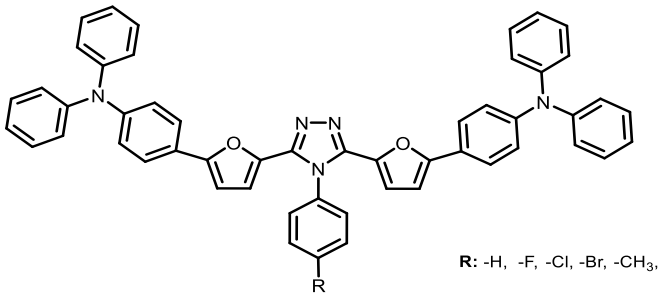


Figure 38. Designed Molecules M1–M5 within the Framework of This Study

Although M1–M5 have not yet been synthesized, computational predictions provide substantial insight into their potential properties. Mulliken partial charge analyses and FMO visualizations confirmed that the electronic distributions of the designed molecules aligned well with design expectations, lending credibility to the computational results. Additionally, insights derived from the previously studied compounds 1–5 offer a valuable reference for anticipating the behavior of the novel molecules. These comparisons support the hypothesis that TPA integration effectively tunes electronic energy levels while maintaining structural stability and favorable geometry.

The influence of the solvent environment on molecular properties was also considered. Solubility is a critical factor in the practical implementation of OPV materials, and both chloroform ($CHCl_3$) and dimethyl sulfoxide (DMSO) were selected as representative solvents due to their substantially different dielectric constants, corresponding to nearly nonpolar and highly polar conditions, respectively. Computational results indicated that solvent polarity exerted negligible influence on the HOMO–LUMO gap and did not substantially alter the charge distribution in the frontier orbitals. This finding confirms that the observed electronic improvements following TPA incorporation are intrinsic to the molecular architecture and are not artifacts of solvent effects.

Overall, the integration of TPA groups into the D–A–D framework of M1–M5 successfully enhanced π-conjugation and significantly reduced the HOMO–LUMO energy gaps, thereby improving their semiconducting potential. The banana-shaped geometry of these molecules, coupled with strategic functionalization, is expected to facilitate favorable intermolecular interactions, efficient π–π stacking, and enhanced charge transport—all critical factors for achieving high-performance OPV devices. The computational results underscore the value of rational molecular design, demonstrating that systematic modulation of electronic properties and molecular geometry can yield NFAs with optimized photovoltaic characteristics.

In conclusion, this study highlights the critical importance of combining rational design principles with computational analyses to develop next-generation small-molecule NFAs for OPV applications. By leveraging the intrinsic stability and planarity of the 1,2,4-triazole core, strategically extending π-conjugation, and introducing electron-donating functionalities such as TPA, M1–M5 exemplify a new class of molecules with potential to achieve high-performance, cost-effective organic solar cells. The findings provide a robust computational foundation for future experimental synthesis and evaluation, offering clear guidelines for balancing electronic properties, molecular geometry, and structural modifications in the rational design of advanced NFAs. As such, M1–M5

represent a promising avenue for the development of efficient, scalable, and commercially viable OPV technologies.

Conclusion

This study presented the theoretical design and comprehensive quantum chemical investigation of a new series of non-fullerene acceptor molecules (M1–M5) based on a 1,2,4-triazole core and a donor–acceptor–donor (D–A–D) architecture. By introducing triphenylamine (TPA) donor units to enhance π-conjugation and promote push–pull electronic effects, the molecular framework was systematically modified to improve electronic properties relevant to photovoltaic applications.

Density Functional Theory (DFT) calculations at the B3LYP/6-31G(d,p) level, combined with TD-DFT/TDA excited-state analyses, demonstrated that the designed molecules possess stable, predominantly banana-shaped conformations and favorable electronic characteristics. In particular, incorporation of the TPA group led to a pronounced reduction in the HOMO–LUMO band gap compared with previously studied parent compounds. For example, the calculated band gap of compound 1 (≈3.9 eV) decreased to 2.62 eV for M1, with similar trends observed for M2–M4. Such narrowing of the band gap shifts these systems from insulating toward semiconducting behavior, a critical requirement for efficient organic photovoltaic materials.

Frequency calculations confirmed the stability of the optimized geometries, while Mulliken charge analyses and frontier molecular orbital distributions supported the intended donor–acceptor electronic structure. The HOMO–LUMO orbitals showed appropriate charge separation characteristics, consistent with enhanced intramolecular charge transfer. Solvent effects ($CHCl_3$ and DMSO), despite their markedly different dielectric constants, were found to exert minimal influence on band gap values and frontier orbital charge distributions, indicating that the electronic properties of these molecules are largely intrinsic to their molecular structures.

Although the M1–M5 molecules have not yet been synthesized, the strong agreement between design expectations, charge distributions, orbital characteristics, and systematic band gap reduction provides confidence in the reliability of the computational approach. The results clearly demonstrate that increasing conjugation and employing TPA-based donor doping is an effective strategy for tuning the electronic structure of 1,2,4-triazole–based systems toward photovoltaic suitability.

Overall, this work advances the rational design of banana-type, fullerene-free organic acceptors and provides a solid theoretical foundation for their future synthesis and experimental evaluation. The proposed molecules represent promising candidates for use in low-cost, high-efficiency organic solar cells, and future studies may focus on experimental realization, device fabrication, and further structural modifications to optimize power conversion efficiency.

Acknowledgements

We sincerely express our profound gratitude to Mr. Abdul Jamil Haidari, Professor in the Department of Inorganic Materials Engineering, and Professor Abdul Qayum Rajabi, Head of the Department of General Chemistry, Faculty of Industrial Chemical Engineering, Jowzjan University, as well as to the respected faculty members of the aforementioned faculty, for their valuable support, guidance, and encouragement throughout the course of this research.

Author Contributions

Abdul Manan Zahir (A.M.Z.) conceptualized the study, designed the molecules (M1–M5), and coordinated data collection, including gathering chemical structures and computational inputs.

Zainullah Matin (Z.M.) performed all quantum chemical calculations, including geometry optimization, frequency analyses, excited-state energy calculations, and evaluation of HOMO–LUMO orbitals and Mulliken charge distributions.

Abdul Jamil Haidari (A.J.H.) assisted with computational methodology, software usage (Gaussian 16 Rev. A.03, GaussView 6.0.16, ChemAxon Marvin Suite, ChemOffice), data validation, and critical manuscript review. All authors contributed to data interpretation, manuscript drafting, and approved the final version for submission.

Funding

No funding is available for the manuscript.

Conflicts of Interest

The authors declare that they have no conflict of interest.

Data Availability

The computational data generated and analyzed during this study, including molecular properties, HOMO–LUMO frontier orbitals, geometry optimizations, Mulliken charge distributions, and excited-state calculations for molecules M1–M5 in the gas phase and in $CHCl_3$ and DMSO solvents, are available from the corresponding author upon reasonable request. All computational analyses were performed using Gaussian 16 Rev. A.03, GaussView 6.0.16, ChemAxon Marvin Suite, and ChemOffice software packages.

References

Aboulouard, A., Mtougui, S., Demir, N., Moubarik, A., Idrissi, M. E., & Can, M. (2021). New non-fullerene electron acceptors-based on quinoxaline derivatives for organic photovoltaic cells: DFT

computational study. *Synthetic Metals*, *279*, 116846. https://doi.org/10.1016/j.synthmet.2021.116846

Akış, M. (2019). Furan Sübstitüe Konjuge Triazol Bileşiklerinin Sentezi Ve Kuantum Kimyasal Hesaplamalari.

ChemAxon. (2019). Marvin Suite [Computer software]. ChemAxon Ltd.

Chen, H. (2019). Electron-deficient core fused-ring based non-fullerene acceptor enables over 15% efficiency in single junction organic solar cells. *Science China Chemistry*, *62*(4), 403–404. https://doi.org/10.1007/s11426-019-9431-8

Chen, H., & Xu, Z. (2018). OLED panel radiation pattern and its impact on VLC channel characteristics. *IEEE Photonics Journal*, *10*(2), 1–10. https://doi.org/10.1109/JPHOT.2017.2774241

Demirci. (n.d.). BAZI Tiyenotiyofenlerin Sentezi Ve Uygulamalari.

Eok Jang, S., Ok Jeon, S., Joo Cho, Y., Soo Yook, K., & Yeob Lee, J. (2010). Stable efficiency roll-off in red phosphorescent organic light-emitting diodes using a spirofluorene–benzofluorene-based carbazole type host material. *Journal of Luminescence*, *130*(11), 2184–2187. https://doi.org/10.1016/j.jlumin.2010.06.017

Frisch, M. J. (2019). Gaussian 16 (Revision A.03) [Computer software]. Gaussian, Inc.

Fu, Y., Lee, T. H., Chin, Y.-C., Pacalaj, R. A., Labanti, C., Park, S. Y., . . . Kim, J.-S. (2023). Molecular orientation-dependent energetic shifts in solution-processed non-fullerene acceptors and their impact on organic photovoltaic performance. *Nature Communications*, *14*(1), 1870. https://doi.org/10.1038/s41467-023-37234-0

Fürk, P., Paarhammer, D., Klimenkovs, I., Savkins, A., Berzins, K., Reinfelds, M., . . . Trimmel, G. (2023). Alkylated Y-series acceptors for ternary organic solar cells with improved open-circuit voltage processed from non-halogenated solvents. *Energy Advances*, *2*(9), 1399–1408. https://doi.org/10.1039/D3YA00163F

He, C., Li, Y., Li, S., Yu, Z.-P., Li, Y., Lu, X., Shi, M., Li, C.-Z., & Chen, H. (n.d.). Near-Infrared Electron Acceptors with Unfused Architecture for Efficient Organic Solar Cells.

Hou, J., Inganäs, O., Friend, R. H., & Gao, F. (2018). Organic solar cells based on non-fullerene acceptors. *Nature Materials*, *17*(2), 119–128. https://doi.org/10.1038/nmat5063

Jiang, K., Wei, Q., Lai, J. Y. L., Peng, Z., Kim, H. K., Yuan, J., . . . Yan, H. (2019). Alkyl chain tuning of small molecule acceptors for efficient organic solar cells. *Joule*, *3*(12), 3020–3033. https://doi.org/10.1016/j.joule.2019.09.010

Kollár, E., Pohl, L., Poppe, A., & Kohári, Z. (2014). Nonlinear electro-thermal and light output modeling and simulation of OLEDs. *Periodica Polytechnica Electrical Engineering and Computer Science*, *58*(2), 43–53. https://doi.org/10.3311/PPee.7477

Lee, J. E., Kim, Y., Na, Y. H., Baek, N. S., Jung, J. W., Choi, Y., . . . Kim, T.-D. (2021). Efficient inverted solar cells using benzotriazole-based small molecule and polymers. *Polymers*, *13*(3), 393. https://doi.org/10.3390/polym13030393

Lee, J., Lee, J.-I., Lee, J. Y., & Chu, H. Y. (2009). Stable efficiency roll-off in blue phosphorescent organic light-emitting diodes by host layer engineering. *Organic Electronics*, *10*(8), 1529–1533. https://doi.org/10.1016/j.orgel.2009.08.020

Lei, Y., Meng, X., Guo, Q., Sun, X., & Zhou, E. (2025). Recently progress of aromatic side chain engineering on Y6 for high performance organic solar cells. *Nano Research*, *18*(10), 94907513. https://doi.org/10.26599/NR.2025.94907513

Li, D., Wei, N., Chen, Y.-N., Wang, X., Han, X., Bian, Z., . . . Bo, Z. (2026). Asymmetric side-group engineering of nonfused ring electron acceptors for high-efficiency thick-film organic solar cells. *Nano-Micro Letters*, *18*(1), 81. https://doi.org/10.1007/s40820-025-01905-y

Liu, S., Yuan, J., Deng, W., Luo, M., Xie, Y., Liang, Q., . . . Cao, Y. (2020). High-efficiency organic solar cells with low non-radiative recombination loss and low energetic disorder. *Nature Photonics*, *14*(5), 300–305. https://doi.org/10.1038/s41566-019-0573-5

Mahmood, A., Yang, J., Hu, J., Wang, X., Tang, A., Geng, Y., . . . Zhou, E. (2018). Introducing four 1,1-dicyanomethylene-3-indanone end-capped groups as an alternative strategy for the design of small-molecular nonfullerene acceptors. *The Journal of Physical Chemistry C*, *122*(51), 29122–29128. https://doi.org/10.1021/acs.jpcc.8b09336

Mahmoud, S. E., Badawy, S. A., Fadda, A. A., Abdel-Latif, E., & Elmorsy, M. R. (2025). Triphenylamine-based metal-free organic dyes as co-sensitizers: Enhancing dye-sensitized solar cell performance through innovative molecular design. *Journal of Fluorescence*, *35*(11), 10925–10938. https://doi.org/10.1007/s10895-025-04340-9

Nielsen, C. B., Holliday, S., Chen, H.-Y., Cryer, S. J., & McCulloch, I. (2015). Non-fullerene electron acceptors for use in organic solar cells. *Accounts of Chemical Research*, *48*(11), 2803–2812. https://doi.org/10.1021/acs.accounts.5b00199

Park, S., Heo, J. H., Yun, J. H., Jung, T. S., Kwak, K., Ko, M. J., . . . Son, H. J. (2016). Effect of multi-armed triphenylamine-based hole transporting materials

for high performance perovskite solar cells. *Chemical Science*, *7*(8), 5517–5522. https://doi.org/10.1039/C6SC00876C

PerkinElmer. (2021). ChemOffice [Computer software]. PerkinElmer Informatics.

Quezada-Borja, J. D., Rodríguez-Valdez, L. M., Palomares-Báez, J. P., Chávez-Rojo, M. A., Landeros-Martinez, L.-L., Martínez-Ceniceros, M. C., . . . Sánchez-Bojorge, N. A. (2022). Design of new hole transport materials based on triphenylamine derivatives using different π-linkers for the application in perovskite solar cells. A theoretical study. *Frontiers in Chemistry*, *10*, 907556. https://doi.org/10.3389/fchem.2022.907556

Rajavelu, K., & Rajakumar, P. (2018). Synthesis and DSSC application of donor-acceptor stilbenoid dendrimers with triphenylamine as core and benzothiazole as surface unit. *Organic Electronics*, *56*, 192–200. https://doi.org/10.1016/j.orgel.2018.02.020

Rezvan, V. H. (2025). Charge transfer complexes: A review survey. *Results in Chemistry*, *17*, 102600. https://doi.org/10.1016/j.rechem.2025.102600

Sharda, S., & Singh, D. (2019). Solar photovoltaic technologies: An approach to sustainable energy. *International Journal of Current Microbiology and Applied Sciences*, *8*(03), 89–99. https://doi.org/10.20546/ijcmas.2019.803.014

Silva, O. K. T. (2024). Solar energy technologies: A complete review of the solar system technologies. *J. Res. Technol. Eng*, *5*(1), 84–111.

Wang, H.-Y., Chen, G., Xu, X.-P., & Ji, S.-J. (2010). Synthesis and characterization of triphenylamine–benzothiazole-based donor and acceptor materials. *Synthetic Metals*, *160*(9–10), 1065–1072. https://doi.org/10.1016/j.synthmet.2010.02.028

Wang, Y., Kan, B., Ke, X., Liu, F., Wan, X., Zhang, H., . . . Chen, Y. (2018). Two thieno[3,2-b]thiophene-based small molecules as bifunctional photoactive materials for organic solar cells. *Solar RRL*, *2*(2), 1700179. https://doi.org/10.1002/solr.201700179

Xie, L., Qiu, D., Zeng, X., Kwok, C. H., Wang, Y., Yao, J., . . . Yu, H. (2025). Tailoring small-molecule acceptors through asymmetric side-chain substitution for efficient organic solar cells. *Science China Materials*, *68*(3), 860–867. https://doi.org/10.1007/s40843-024-3252-3

Xie, R., Ying, L., Liao, H., Chen, Z., Huang, F., & Cao, Y. (2018). Efficient non-fullerene organic solar cells enabled by sequential fluorination of small-molecule electron acceptors. *Frontiers in Chemistry*, *6*, 303. https://doi.org/10.3389/fchem.2018.00303

Xu, X., Qi, Y., Luo, X., Xia, X., Lu, X., Yuan, J., . . . Zou, Y. (2023). Alkyl side chain engineering enables high performance as-cast organic solar cells of over 17% efficiency. *Fundamental Research*, *3*(4), 611–617. https://doi.org/10.1016/j.fmre.2022.01.025

Yang, M., Wei, W., Zhou, X., Wang, Z., & Duan, C. (2022). Non-fused ring acceptors for organic solar cells. *Energy Materials*, *1*(1), 100008. https://doi.org/10.20517/energymater.2021.08

Yin, Z., Guo, X., Wang, Y., Zhu, L., Chen, Y., Fan, Q., . . . Li, Y. (2022). Siloxane-functional small molecule acceptor for high-performance organic solar cells with 16.6% efficiency. *Chemical Engineering Journal*, *442*, 136018. https://doi.org/10.1016/j.cej.2022.136018

Yuan, S., Luo, W., Xie, M., & Peng, H. (2025). Progress in research on organic photovoltaic acceptor materials. *RSC Advances*, *15*(4), 2470–2489. https://doi.org/10.1039/D4RA08370A

Zhang, Z., Yuan, J., Wei, Q., & Zou, Y. (2018). Small-molecule electron acceptors for efficient non-fullerene organic solar cells. *Frontiers in Chemistry*, *6*, 414. https://doi.org/10.3389/fchem.2018.00414

Zhao, J., Du, X., Zheng, C., He, Z., Guo, J., Zhang, N., . . . Tao, S. (2020). Reducing efficiency roll-off of phosphorescent organic light emitting diodes by using phosphor assisted energy funneling. *Organic Electronics*, *87*, 105985. https://doi.org/10.1016/j.orgel.2020.105985